Lawrence Berkeley Laboratory
UNIVERSITY OF CALIFORNIA

Physics Division

Invited talk presented at the XV Symposium on Multiparticle Dynamics, Lund, Sweden, June 10-16, 1984

QUARK FRAGMENTATION IN e^+e^- ANNIHILATION

A. Barbaro-Galtieri

September 1984

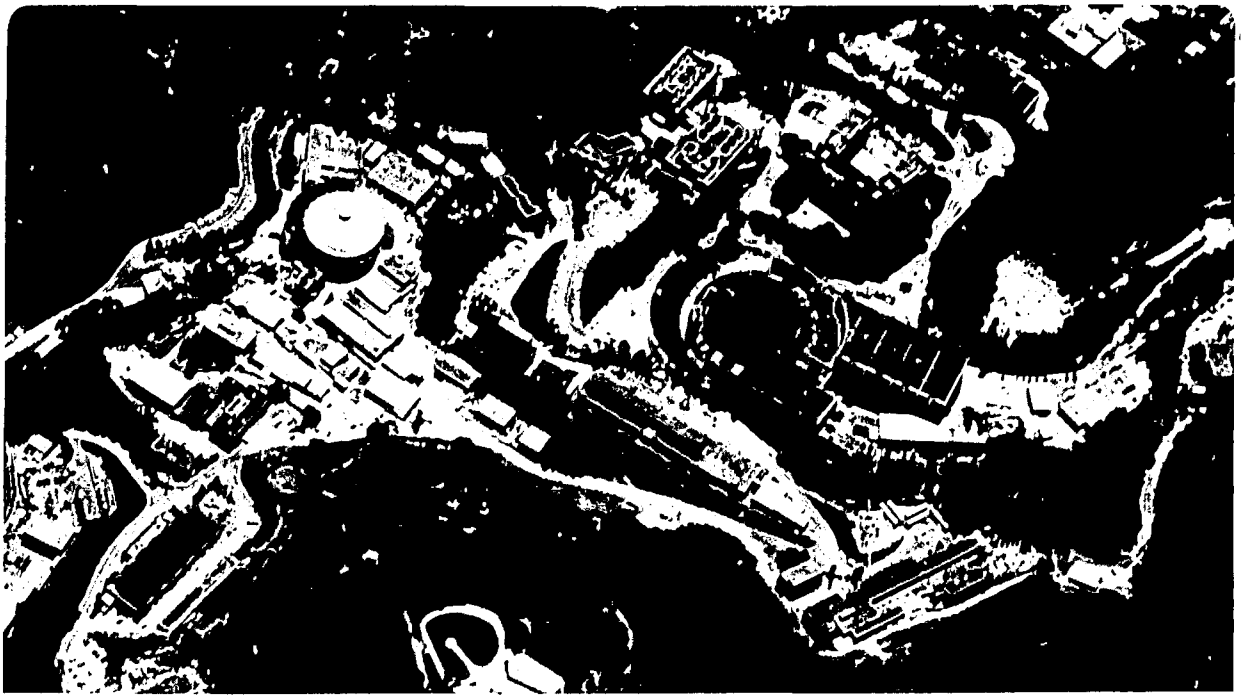

Prepared for the U.S. Department of Energy under Contract DE-AC03-76SF00098

DISCLAIMER

LBL-18424
Invited talk presented at the XV Symposium on Multiparticle Dynamics, Lund, Sweden June 10-16, 1984

Quark Fragmentation in e^+e^- Annihilation*

A. Barbaro-Galtieri
Lawrence Berkeley Laboratory
University of California
Berkeley, CA 94720

Contents

* This work was supported by the U.S. Department of Energy under Contract No. DE-AC03-76SF000098.

1 INTRODUCTION

Jet formation in e^+e^- annihilation was first observed in 1975 at SPEAR by the LBL-SLAC Collaboration at 7 GeV c.m. energy[1]. The data indicated that the hadrons produced in this process emerge in two collimated jets travelling in opposite directions. This is expected in a quark-parton model picture in which the process observed is $e^+e^- \rightarrow q\bar{q}$, with quarks later fragmenting into observable hadrons collimated along the original quark direction. As the c.m. energy increased to 27 GeV in 1979, PETRA experiments[2] observed a new phenomenon, i.e., jets produced by yet another parton: the gluon predicted by QCD.

Our present understanding of jet formation can be pictured as follows. The initial e^+e^- annihilate into an energetic virtual photon that creates the initial $q\bar{q}$. The two color-carrying quarks separate in space and emit gluons according to perturbative QCD. New $q\bar{q}$ pairs are produced which at a later stage produce colorless hadrons.

Over the past few years many models have been developed to describe the different steps that bring about hadron production in jets. The early Feynman and Field[3] model and its extensions[4-5] explain most of the e^+e^- data. This model is generally referred to as the 'independent fragmentation' (IF) model. A widely used and successful model is the 'color string fragmentation' or LUND model[6] that seems to fit a large class of data not only in e^+e^- but also in leptoproduction and hadron collisions. Recently, 'QCD-Cluster' models have been developed and Monte Carlo programs have been written as a convenient way to study parton showers and for comparison with the data[7-8]. The Webber[9] and Gottschalk[10] models belong to this class.

The conventional models, IF and LUND, assume that jets are a non-perturbative phenomenon that is governed by confinement forces. In the IF model[3] a fast quark picks up a $q\bar{q}$ pair and emits a meson ($q \rightarrow M + q'$) in a recursive cascade process until all energy is used up. In the extension by Hoyer et al.[4] and Ali et al.[5], hard gluon radiation is emitted by the primary quarks according to perturbative QCD and the gluon then creates its own jet. In the LUND model, a string color field stretching between the separating color quarks produces $q\bar{q}$ pairs that screen the color field. These $q\bar{q}$ pairs eventually recombine into mesons. The gluon is a kink in the string: each section of the string fragments separately resulting in three separate jets.

In 'QCD-Cluster' models the initial quarks undergo successive gluon emissions according to perturbative QCD, the gluons in turn emit further gluons or convert into $q\bar{q}$ pairs creating a parton shower. In the final step color-singlet 'clusters' are formed from which hadrons are produced non-perturbatively. Their mass scale is controlled by a cut-off Q_0 at which the parton shower is ended. The main difference between the two types of models is the scale at which perturbative effects are ended: in conventional models the cut-off is large ($Q^2 = 20 - 100$

GeV^2); in parton shower models QCD is used down to $Q^2 \sim 1$ GeV^2 for the Webber model[9]. The Gottschalk model[10] uses a Q^2 cut-off somewhere in between ($t_c \sim 15$ GeV^2) and parameterizes the decays of clusters into hadrons according to observed hadronization at low energies.

In this report experimental data that provide information on parton fragmentation are reviewed. Heavy quark fragmentation will not be discussed, since it is covered by J. Izen in a separate report. The data will be compared with the models outlined above, the LUND model being used more often.

The general features of the data are well described by all models. Differences between independent fragmentation and string fragmentation appear clearly in detailed studies of three-jet events as first reported by JADE[11]. The string fragmentation model fits the data better. A surprising result presented at this Conference is that the Webber model also predicts string-like effects.

2 INCLUSIVE HADRON PRODUCTION

Detailed studies of the composition of jets and production properties of particles in jets are essential to understand the dynamics of jet evolution from the $q\overline{q}$ pair to the final hadrons. Of course, all we can see are the final hadrons, therefore the interesting region of confinement and perturbative QCD has to be disentangled from non-perturbative effects like resonance or cluster decays. In this section we will review the data available on properties of jets: particle type composition and spectra, rapidity and $p_\perp$ distributions.

2.1 Jet Properties

The first step towards an understanding of jet formation is the study of particle yields and particle spectra. These studies are important to determine the parameters of the models, so that their adequacy to fit a large body of data can be tested.

Particle yields provide information on multiplicities of $q\overline{q}$ pairs pulled from the vacuum, on the type of pairs (i.e. u:d:s ratio), on the ratio of diquark to quark pairs (relevant to one model of baryon production) and also on how many vector versus pseudoscalar particles (V/P ratio) are produced in the hadronization phase. For conventional models these ratios are tunable parameters, whereas for the QCD-Cluster models they do not explicitly enter as parameters.

Particle spectra provide information on the fragmentation function, $D(x)$. The spectra are usually presented in distributions like

$$D(x) = (1/\sigma\beta)d\sigma/dx \qquad (1)$$

with $x = 2E_h/\sqrt{s}$ (different variables are used by different experiments, $x_p = 2p/\sqrt{s}$ is often used) and β is the velocity of the particle. $D(x)$ represents then

the particle density produced at x in a unit interval of x. Again for the conventional models some tunable parameters are available to fit the fragmentation functions. For the QCD-Cluster models fragmentation functions do not enter explicitly, therefore particle spectra and yields are used to fit the tunable parameters. For the Webber model[9] these are Λ (QCD scale), Q_0 (gluon mass cut-off) and M_f (cluster mass above which clusters do not decay isotropically). For the Gottschalk model[10] some of the parameters are: Λ (QCD scale), t_c (mass squared cut-off for resolvable radiation), W_{max} (cluster mass above which the clusters are broken into smaller clusters using the string formalism), ρ_c (the string strength) and W^c_{min} (the minimum cluster mass).

In this section the available data on stable particles and on resonance production will be reviewed.

2.1.1 Stable Particle Production

The total charged particle multiplicity at $E_{cm} = 29$ GeV has been measured by HRS[12] at PEP to be $n_{ch} = 13.10 \pm 0.05 \pm 0.6$. At $E_{cm} = 34.5$ GeV TASSO[13] finds $n_{ch} = 13.48 \pm 0.03$. The scaled cross sections $s d\sigma/dz$ (where $z = p/E_{beam}$) for these two experiments is shown in Fig. 1. The agreement is very good in the overlap region. The HRS data extend to higher z values, where light quarks are the major contributors. The momentum resolution of the HRS detector is $0.1\%\ p$ (in GeV/c), which allows studies of $D(z)$ in the very interesting region $z \rightarrow 1$. These results are discussed in the talk by M. Derrick.

A large fraction of the charged particles produced in the jets are pions, mostly decay products of resonances. The multiplicities, as measured by various experiments, are shown in Table 1. The normalized cross sections versus x for pions, kaons, and protons, as measured by the TPC[14] at PEP are shown in Fig. 2. The insert shows a comparison with the $K^{\pm}$ results of the TASSO experiment[15] at $\sqrt{s} = 34$ GeV. There is a clear disagreement for $x \leq 0.1$, which is also reflected in the charged kaon multiplicities shown in Table 1, where $N_K\pm = 1.35 \pm 0.13$ for TPC and 2.0 ± 0.2 for TASSO. Two different techniques of particle identification are used by the two experiments (TPC used dE/dx measurements, TASSO used time of flight) so the systematics are quite different. In Fig. 2 the curves are calculated using the LUND model[6].

The baryon production mechanism included in the LUND model assumes that a fraction of the time a diquark-antidiquark pair is produced in the color field rather than a quark-antiquark pair. The diquark pair then combines with a quark to form a baryon. The parameters used are as follows: s/u probability ratio $P(s)/P(u) = 0.3$, and diquark to quark probability $P(qq)/P(q) = 0.09$. Curves calculated using the 'Independent Fragmentation' model[3-5] fit equally well. The Webber model[9] predicts a multiplicity $N_K\pm = 1.34$, in agreement with the TPC result, and a slightly softer kaon distribution (see Sec. 2.2.1). The Gottschalk

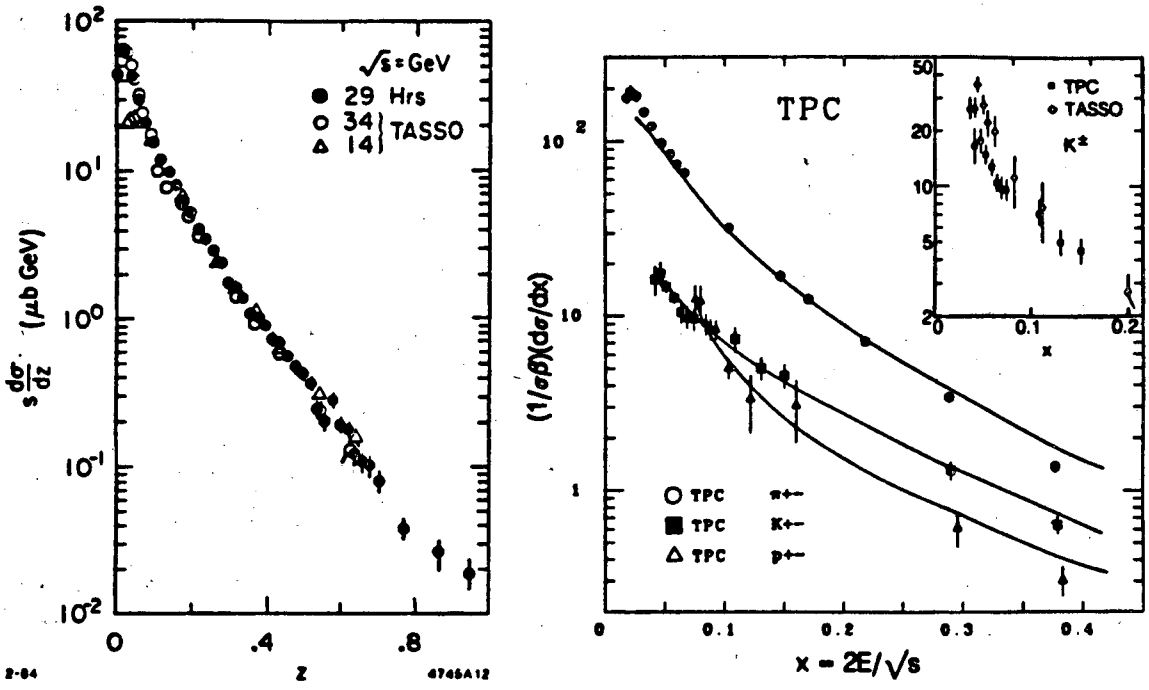

Figure 1: Inclusive scaled cross section for charged hadron production versus $z = 2p/\sqrt{s}$ as measured by HRS[12] and by TASSO[13].

Figure 2: TPC normalized cross section versus x for pions, kaons and protons at $\sqrt{s} = 29$ GeV[14]. The inset shows a comparison with TASSO[15]. The curves are calculated using the LUND Model.

model with the present parameters[10] predicts too few baryons (see Sec. 2.1.3).

What else can we learn from charged particle inclusive distributions? The low x region can be used to test the effects of soft gluon interference predicted by perturbative QCD[16] and included in the Webber Monte Carlo[17,9]. This interference leads to strong suppression of soft partons and consequently of soft hadrons in jets. A specific prediction is that the inclusive cross section $(x_p/\sigma)(d\sigma/dx_p)$ (with $x_p = 2p/\sqrt{s}$) can be described as a Gaussian in $ln(x_p)$ and that the position of the peak shifts to larger values of x_p for heavier masses. This normalized cross section as measured by the TPC for kaons and protons is shown in Fig. 3. The dashed curves have been calculated by the Webber Monte Carlo[9]. The data are consistent with a Gaussian shape, the peaks are approximately where they are expected and move to larger values of x_p for protons. However, the LUND model[6] (solid lines), also provides a good description of the data. These distributions do not permit distinction between the two models. Monte Carlo studies show that they also predict similar energy dependence.

Neutral particle cross sections have also been measured. Figure 4 is a compilation of π^0 and η normalized cross sections versus x. The TPC data on

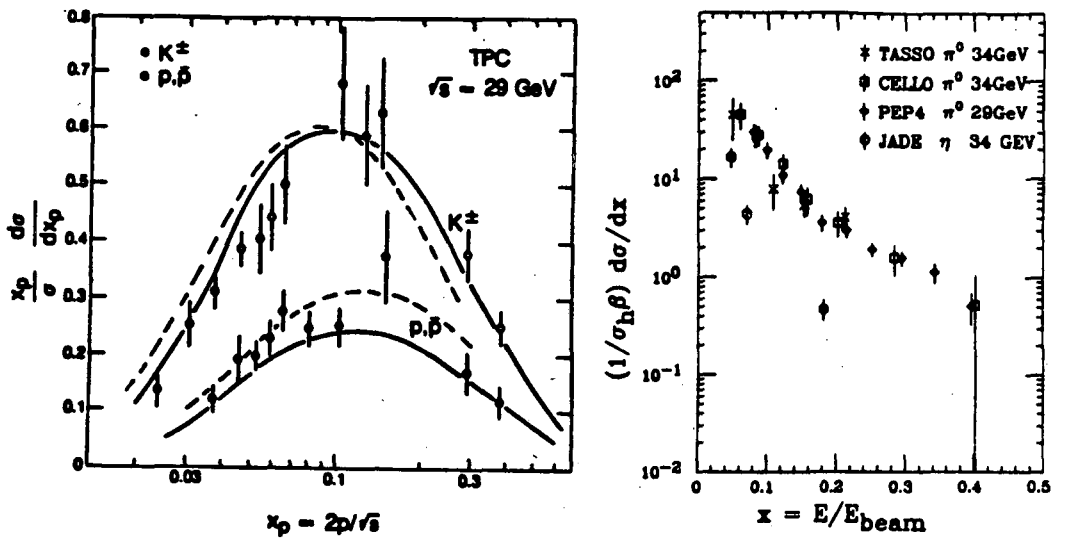

Figure 3: Inclusive cross section $(x_p/\sigma)(d\sigma/dx_p)$, where $x_p = 2p/\sqrt{s}$, as measured by TPC[14]. The curves represent the predictions of the Webber Monte Carlo[9] (dashed) and of LUND (solid lines)[6].

Figure 4: Neutral pion normalized cross section as measured by TASSO, CELLO[19] and TPC[18]. The JADE[20] results on η production are also shown.

π^0 have been reported recently[18] and are in agreement with earlier results by TASSO and CELLO[19]. There is good agreement between the π^0 and $\pi^\pm$ distributions. The TPC measures $r = 2\sigma_0/(\sigma_+ + \sigma_-) = 0.92 \pm 0.14$ for $x = 0.08 - 0.41$, TASSO reports $r = 1.2 \pm 0.4$ for $x = 0.03 - 0.09$. As for η production, the JADE results[20] are shown in Fig. 4. Table 1 summarizes the particle multiplicity measured in these experiments. The LUND and Webber model predictions are in good agreement with these measurements (see later). A compilation of the K^0 cross sections reported by JADE[21] at many energies and the newer TPC data[22] is shown in Fig. 5. Table 1 summarizes the multiplicities as measured by many experiments. Again the agreement among the results is reasonable. The multiplicity as measured by the TPC ($N_{K^0} = 1.22 \pm 0.03 \pm 0.15$) is smaller than that of TASSO ($N_{K^0} = 1.6 \pm 0.1$), but it is in agreement with the TPC measured charged kaon multiplicity ($N_{K^\pm} = 1.35 \pm 0.13$) and with the MARK II[31] result ($1.27 \pm 0.03 \pm 0.15$).

We now turn to measurements related to baryon production. In addition to the proton spectra, already discussed, both Λ and Ξ production have been studied. These three baryons have different quark composition and their production rates are related in some models to tunable parameters. The diquark model for baryon production[23] expects the proton $[u(ud)]$ and the $\Lambda[u(sd)]$ rates to be related by the $(sd)/(ud)$ ratio. In addition the $\Xi[s(sd)]$ should be related to the Λ rate by the s/u ratio. Both the Independent Fragmentation model[24] and the LUND model

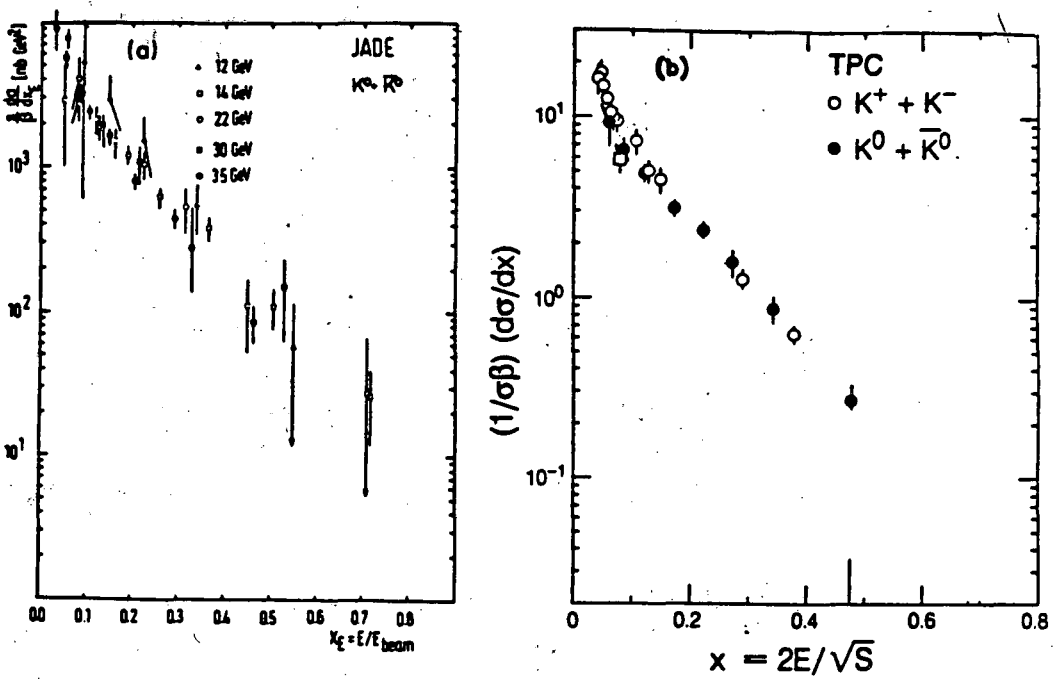

Figure 5: Results on K^0 production. (a) scaled cross section from JADE[21] in the $\sqrt{s}$ = 12 to 35 GeV range. (b) the TPC[22] normalized cross section compared with charged kaons[14].

have these ratios as tunable parameters. A compilation of Λ spectra as measured by TASSO, JADE[25] and TPC[26] is shown in Fig. 6. The measured multiplicities are shown in Table 1. TPC has also recently observed 16 ± 4 events at the Ξ thus confirming an earlier observation by TASSO[27].

Figure 7 shows the differential cross sections for protons, Λ and Ξ as measured by the TPC. The curves are again obtained with the LUND model[6]. The values of the relevant parameters are:

$$R = \frac{P(qq)}{P(q)} = 0.085 \qquad r = \frac{P(su)}{P(ud)} \cdot \frac{P(d)}{P(s)} = 0.4$$

where $P(qq)$ and $P(q)$ are the probabilities to produce a diquark or a quark pair, respectively. For r, the extra strange-diquark suppression factor, the flavors are explicitly indicated. The values of these parameters are different from the default values of the LUND program ($R = 0.09$, $r = 0.2$), but they are not the result of an overall fit. TASSO[27], using an older version of the LUND model and $s/u = 0.4$, obtains $R = 0.11$, $r = 0.3$. The data are still not sufficient to determine the parameter r accurately, $r = 0.2 - 0.4$ can easily be accomodated by the data.

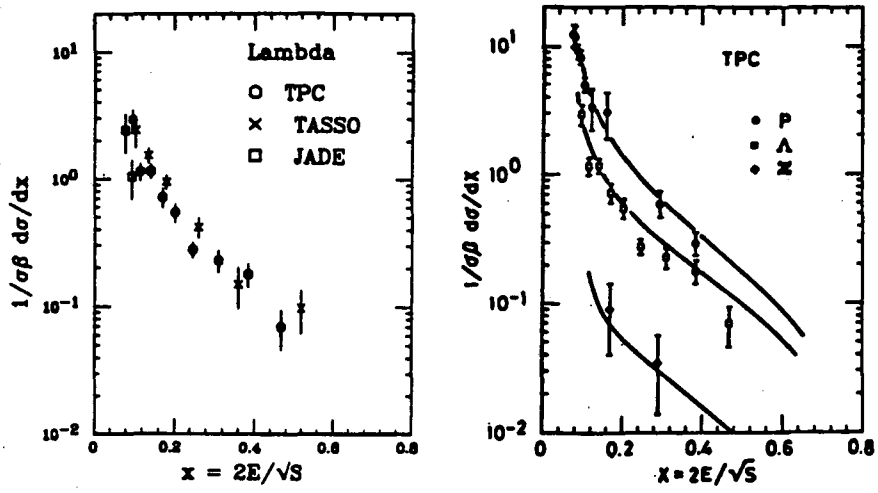

Figure 6: A compilation of Λ normalized cross sections as measured by JADE,[25] TASSO,[25] and TPC[26].

Figure 7: Baryon normalized cross sections as measured by the TPC[14,26]. The curve is calculated with the LUND model.

2.1.2 Resonance Production

The investigation of resonance production in e^+e^- annihilation provides important information on parton fragmentation. Most of the stable particles we have discussed in the previous paragraphs are decay products of resonances, and therefore they are one more step removed from the original partons. The fraction of vector mesons produced, V/P ratio, is a parameter in some models[4-6], therefore, it is important to determine it from the data. In addition, the mass spectrum of hadrons produced in the hadronization process can be approximately predicted in some models[9-10] and therefore it is important to try to measure it.

Since the results on ρ production by the TASSO collaboration[28], new data on vector meson production have become available this last year. Results on K^{*0} and ϕ production are reported by TPC[22,29] and by DELCO,[30] on K^{*0} and ρ production by the MARK II[31] and on $K^{*\pm}$ and ρ by JADE[32].

Some results for the TPC[22,29] and DELCO[30] on K^* and ϕ production are shown in Fig. 8. Both experiments use particle identification to select kaons and the resonances appear as clear peaks in the invariant mass plots without background subtraction. The TPC identifies particle species by combining measurements of energy loss (dE/dx) and momentum. For kaons the average purity of the sample is 70%, for pions 90%. In a 69 pb^{-1} sample of data the $K\pi$ and KK invariant mass plots of Fig. 8a-b are obtained. Fits with the sum of a Breit-Wigner shape folded with the detector resolution and a smooth background to the 'unlike signs' distributions yield 2250±120 K^* events and 62±11 ϕ events. The r.m.s. width for the ϕ peak in Fig. 18b is 6.2±0.4 MeV, consistent with the

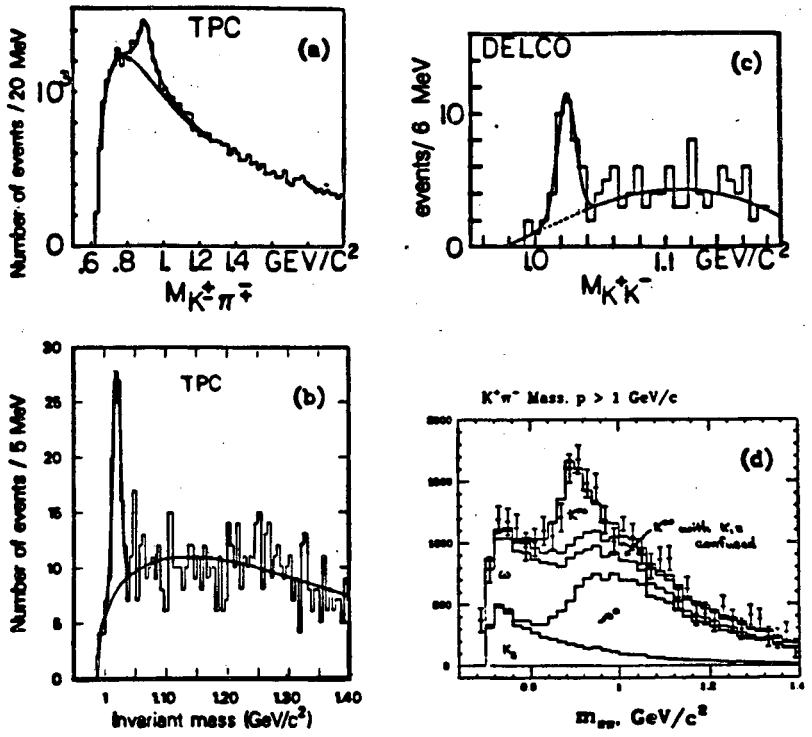

Figure 8: Vector meson production data. (a) $K^\pm\pi^\mp$ invariant mass from the TPC[22]. (b) and (c) K^+K^- invariant mass from TPC[29] and DELCO[30]. (d) Background subtracted $\pi^-\pi^-$ invariant mass from MARK II[31]; the contributions from the individual states are shown.

detector resolution. The scaled inclusive cross sections versus x $(= 2E/\sqrt{s})$ for K^* and ϕ production are shown in Fig. 9a. The particle yields per event are shown in Table 1.

The DELCO results on ϕ production[30] are shown in Figs. 8c and 9a. A sample of 92 pb^{-1} of data has been used. The kaons are identified above 2.5 GeV/c by a Cerenkov counter filled with isobutane with a pion threshold at 2.5 GeV/c. Figure 8c shows the invariant K^+K^- mass distribution obtained when both tracks are identified by the Cerenkov counter. An enhancement is observed at the ϕ mass, containing 26 ϕ's with an estimated background of 14 events. The width of the peak is $\sigma = 10$ MeV, consistent with the resolution. The K^{*0} peak (not shown) is not as background free as the ϕ peak. Here the kaon was required to have a momentum above 3.2 GeV/c to reduce pion contamination. No particle identification is required for the second track. The x region covered is $0.216 \leq x \leq 0.830$ for the K^{*0} and $0.35 \leq x \leq 0.8$ for the ϕ. The values obtained for the scaled cross section are plotted in Fig. 9a and are in agreement with the TPC data.

The K^{*0} and ϕ normalized cross sections are compared with the TPC $K^\pm$ data in Fig. 9a. The curves have been calculated with the LUND model[6]. They agree with the data reasonably well. The K^{*0} and ϕ curves exhibit a flatter

Table 1: Particle yield measured at PEP and PETRA in e^+e^- collisions in the $\sqrt{s} = 29 - 34.5$ GeV range. All stable particles include the decay products of short lived particles ($\tau \leq 5 \times 10^{-10}$ sec) and of resonances.

Particle	Particles/Event	Experiment	Ref.	Remarks
$\pi^{\pm}$	10.7 ± 0.6	TPC	14	
	10.3 ± 0.4	TASSO	15	
π^0	6.1 ± 2.0	TASSO	19	
	5.2 ± 1.8	CELLO	19	
	5.3 ± 0.7	TPC	18	
η	$0.72 \pm 0.10 \pm 0.18$	JADE	20	
ρ^0	0.73 ± 0.06	TASSO	28	
	$0.436 \pm 0.043 \pm 0.057$	MARK II	31	$x = 0.07 - 0.7$[a]
	$0.98 \pm 0.09 \pm 0.15$	JADE	32	
$K^{\pm}$	1.35 ± 0.13	TPC	14	
	2.0 ± 0.2	TASSO	15	
$K^0 + \overline{K}^0$	1.6 ± 0.1	TASSO	21	
	$1.45 \pm 0.08 \pm 0.15$	JADE	21	
	$1.22 \pm 0.03 \pm 0.15$	TPC	22	
	$1.27 \pm 0.03 \pm 0.15$	MARK II	31	
$K^{*\pm}$	$0.87 \pm 0.16 \pm 0.08$	JADE	32	
$K^{*0} + \overline{K}^{*0}$	$0.49 \pm 0.04 \pm 0.07$	TPC	22	$x = 0.061 - 0.8$
	$0.415 \pm 0.045 \pm 0.075$	MARK II	31	$x = 0.07 - 0.7$
ϕ	$0.084 \pm 0.013 \pm 0.018$	TPC	29	
D^0	(0.45 ± 0.12)[b]	HRS	33	
D^+	(0.40 ± 0.10)[b]	HRS	33	
$D^{*\pm}$	$0.39 \pm 0.08 \pm 0.14$	TASSO	33	$x > 0.03$
	(0.34 ± 0.11)[b]	HRS	33	
	$(0.48 \pm 0.08 \pm 0.10)$[b]	JADE	33	
$F^{\pm}$	$(0.015 \pm 0.003 \pm 0.005)/B$	TASSO	34	$x > 0.3$ $B = BR(F \rightarrow \phi\pi)$
$p + \overline{p}$	0.60 ± 0.08	TPC	14	
	0.8 ± 0.1	TASSO	15	
$\Lambda + \overline{\Lambda}$	$0.197 \pm 0.012 \pm 0.018$	TPC	26	
	0.28 ± 0.04	TASSO	25	
$\Xi^{\pm}$	$0.025 \pm 0.009 \pm 0.008$	TPC	26	
	$0.026 \pm 0.008 \pm 0.009$	TASSO	27	

[a] In this x interval the TASSO and JADE results agree with the MARK II results

[b] Calculated by us, using $R_h = 4.0$. D rates include decay products from D*.

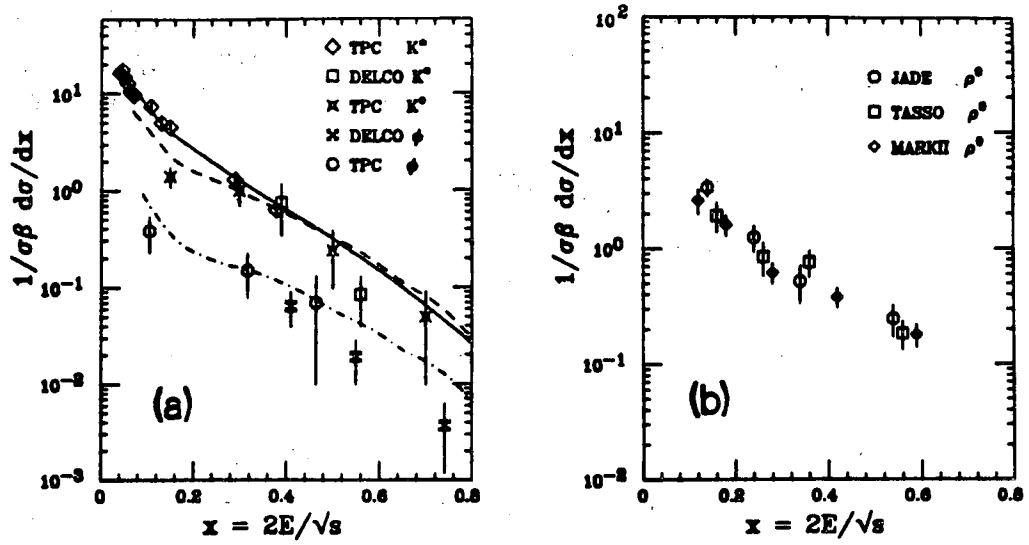

Figure 9: Normalized cross sections for vector meson production. (a) Results on K^{*0} and ϕ production from the TPC[22,29] and DELCO[30] compared with the TPC[14] $K^{\pm}$. (b) The TASSO,[28] JADE[32] and MARK II[31] results on ρ^0 production.

distribution at large x. This is expected since most of the kaons are decay products of resonances, hence have lower momenta than the resonances themselves.

JADE[32] has measured the cross section versus x for $K^{*\pm}$ production detected via the decay $K^{*\pm} \rightarrow K^0_s\pi^{\pm}$. They obtain fewer events than for K^{*0}, but the signal to background ratio is larger. The number of $K^{*\pm}$ per event, integrated over the whole x region, is shown in Table 1.

We now turn to ρ^0 production as reported by JADE[32] at $\sqrt{s} = 34$ GeV and by MARK II[31] at $\sqrt{s} = 29$ GeV. These experiments do not use particle identification, so the '$\pi^+\pi^-$' invariant mass has also contributions from K^{*0} and other $K\pi$ combinations. The technique used by JADE[32] is to fit the $\pi^+\pi^-$ mass after subtraction of a smooth background, estimated by fitting the like-sign pairs. MARK II[31] considers each track alternatively as a kaon or pion and simultaneously fits the two distributions with smooth backgrounds and contributions from known states. TASSO[28] has used both methods which give similar results. For all three experiments the states included are K^0_s, K^{*0}, ω and ρ^0.

Figure 8d shows the MARK II background-subtracted '$\pi^+\pi^-$' invariant mass with the individual contributions. Because of the simultaneous fit, MARK II can also give results on the K^{*0}. After acceptance correction they obtain for $x = 0.07 - 0.7$:

$$\frac{\sigma(K^*)}{\sigma(\rho)} = 0.96 \pm 0.14 \pm 0.17$$

The number of ρ and K* per event for this x range is shown in Table 1. Figure 9b shows the ρ^0 scaled cross section as obtained by MARK II[31] at $\sqrt{s} = 29$ GeV and by TASSO[29] and JADE[32] at $\sqrt{s} = 34$ GeV. The integral of the TASSO and JADE data over the whole x range is shown in Table 1. For the range $0.1 \leq x \leq 0.7$, where the measurements were made, they obtain:

$$N_\rho = 0.41 \pm 0.04 \pm 0.08 \quad \text{TASSO}$$
$$N_\rho = 0.58 \pm 0.05 \pm 0.09 \quad \text{JADE}$$

in good agreement with the MARK II result, shown in Table 1.

2.1.3 Summary: comparison with fragmentation models

Table 1 is a compilation of yields of particle type per event measured by experiments at PEP and PETRA. Stable particle yields include decay products of resonances and of short lived particles like $K^0_s \to \pi^+\pi^-$, etc. Mesons from heavy quarks (D's, D*'s and F's), are included for completeness[33-34]. The results on heavy quark production are discussed by J. Izen at this Conference. The expected multiplicities for the models we have been using are as follows:

	LUND[6]	Webber[9]	Gottschalk[10]
$\pi^\pm$	10.11	10.00	11.27
π^0	5.85	5.90	6.06
$K^\pm$	1.43	1.34	1.37
K^0	1.44	1.28	1.42
ρ^0	0.89	0.67	0.49
$K^{*\pm}$	0.61	0.54	0.43
K^{*0}	0.64	0.52	0.39
ϕ	0.10	0.087	0.06
p	0.68	0.66	0.26
Λ	0.206	0.350	0.075
Ξ	0.010	0.050	0.0030

These models, with a few adjustable parameters, adequately describe the particle composition of jets. As already mentioned, the Gottschalk model, which is still being tuned and improved, at this point underestimates baryon production (see also Sec. 2.2.1), as pointed out by the author[10]. For the LUND model on the average ~ 6 $q\bar{q}$ pairs, in addition to the two primary ones, are created in the string color field. For the Webber model on the average 5.3 clusters are formed from the parton shower, including subsequent decays of heavy quark clusters and string breaking of clusters with $M \geq M_J$.

The fragmentation functions $D(x)$ have been measured for all the particles in Table 1. The models with a few exceptions reproduce these distributions quite

well. Measurements of $D(x)$ for resonant states (K^{*0}, $K^{*\pm}$, ϕ and more data on ρ) have been reported mostly during this last year. There is an indication that these spectra are harder than the stable particle spectra, as expected since stable particles are mostly decay products of resonances.

Multiplicities and spectra have been used to determine some parameters of the fragmentation models. Specifically for the conventional models the parameters s/u and $P/(P+V)$ have been measured by many experiments as follows:

$P(s)/P(u)$	$0.27 \pm 0.03 \pm 0.05$	JADE[21]	(K^0)
	$0.37 \pm 0.15 \pm 0.08$	TPC[22]	(ϕ, K^*)
	0.40	TASSO[15]	$(K^{\pm}, K^0)$
$P/(P+V)$	$0.42 \pm 0.08 \pm 0.15$	TASSO[28]	(ρ^0)
	$0.49 \pm 0.10 \pm 0.15$	JADE[32]	(ρ_0)
	$0.30 \pm 0.15 \pm 0.11$	JADE[32]	$(K^{*\pm})$
	$0.53 \pm 0.11 \pm 0.09$	TPC[22]	$(K^{*0}, K^{\pm}, K^0)$

where the first error is statistical, the second systematic. The particles in parentheses indicate the type of data used.

The values of these parameters are dependent upon the method used. The JADE parameters were obtained by tuning the LUND Monte Carlo; the TASSO results by tuning the IF model; the TPC parameters by evaluating the contribution of secondaries in the measured rates for the different particles. With the first method the uncertainties on the decay branching ratios used by the LUND or IF models are not included in the systematic errors.

Figure 10 is a compilation of light and heavy quark results for the P/V ratios as presented by JADE[32] (the TPC point has been added by us). The ratios are plotted as a function of the vector and pseudoscalar particle mass ratios, M_V/M_P, as it has been suggested that there could be such a dependence[6]. The relation used for the fitted curve is:

$$P/V = \frac{1}{3}\left(\frac{M_V}{M_P}\right)^{\alpha}$$

where the 1/3 comes from spin factors and α was found to be $\alpha = 0.5 \pm 0.1$.

Baryon production results provide information on other parameters: the diquark to quark ratio and the extra strange quark suppression factor. TPC, using the 'Symmetric' LUND model obtains:

$$R = \frac{P(qq)}{P(q)} = 0.085 \qquad r = \frac{P(su)}{P(ud)} \cdot \frac{P(d)}{P(s)} = 0.2 - 0.4$$

the data are still insufficient to determine r. TASSO[27], using an older version of the LUND model obtains $R = 0.11$, $r = 0.3$.

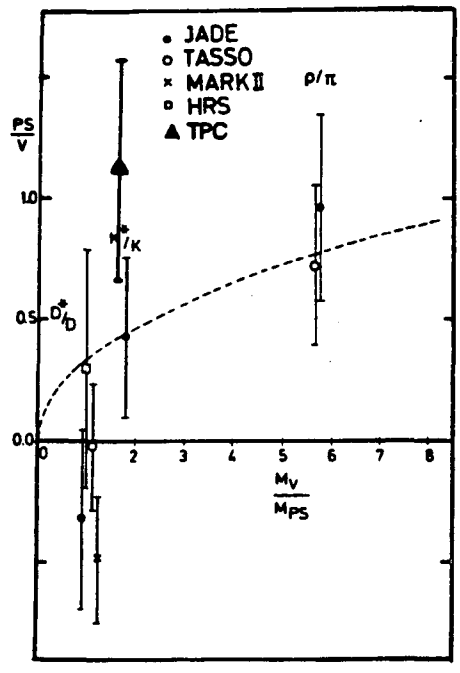

Figure 10: Compilation of pseudoscalar to vector ratios versus the mass ratios taken from JADE[32]. The TPC point[22] has been added.

The Webber model does not use any of the above parameters[9]. The clusters with a mass $M \geq M_f$ (the peak of the cluster mass distribution is at ~ 1 GeV) are broken into smaller clusters using the string formalism, then the final clusters are decayed isotropically in quasi-two-body decays picking up a new quark or diquark pair. The $u/d/s$ ratio is set to 1 and so is the qq/q ratio. In the decay of clusters the resonance spectrum is used ($J^P = 0^-, 1^\pm, 2^+$ for mesons and $J^P = 1/2^+, 3/2^+$ for baryons) and the suppression of strange particles or baryon production is a consequence of reduction of phase space for these channels. Similarly P/V is not an explicit parameter: the spin factors are introduced and phase space takes care of the rest. The agreement with the measured multiplicities is remarkable.

For the Gottschalk model also, the tunable parameters are of a different nature[10]. The clusters made from the parton shower have a higher average mass than those of Webber. These clusters are mostly broken, using the string model formalism, into softer clusters that are then hadronized through the use of a parameterization of low energy data. The physics behind this parameterization is two-body dominance, phase space, statistical particle densities and Zweig's rule.

2.2 More on Quark Fragmentation

In the previous section we have discussed multiplicities and x $(= 2E_h/\sqrt{s})$

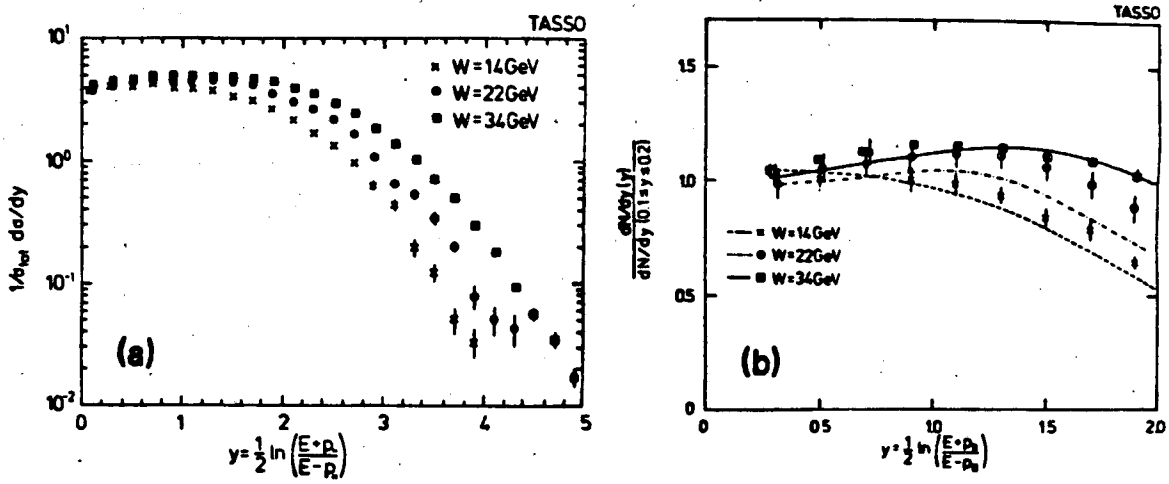

Figure 11: Rapidity measurements by the TASSO collaboration[13]. All charged particles are assigned the pion mass. (a) normalized to σ_{tot}, (b) normalized to the interval $y = 0.1 - 0.2$. The curves are calculated with the LUND model[6].

distributions of different particles. We now try to separate the information on longitudinal and transverse fragmentation by discussing distributions of momentum along the jet axis and perpendicular to it. For conventional models these two fragmentations are introduced separately. For the QCD-cluster models there is no factorization: the transverse momentum distributions arise naturally from the adopted hadronization scheme. We discuss here only recent results that offer some insight on quark fragmentation.

2.2.1 Rapidity Distributions

Particle production along the jet axis can be studied in terms of rapidity

$$y = \frac{1}{2} ln \left(\frac{E + p_L}{E - p_L} \right)$$

where p_L and E are the particle momentum along the jet axis and its energy, respectively.

Figure 11 shows rapidity distributions at different energies as measured by TASSO[13]. No particle identification is used, each particle is assumed to have the pion mass. Rapidity is measured with respect to the thrust axis, the data are folded with respect to $y = 0$. As expected, the distributions are wider at large energies and the so called 'plateau' broadens with increasing energy. The feature that we want to point out here, however, is the dip at $y = 0$. The central region, $y \leq 2$, is shown in Fig. 11b. Here the dip is more visible for the high energy data.

The curves are the prediction of the LUND model[6]. The authors point out that an IF model[3-5] calculation does not reproduce the dip at $y = 0$.

What is the dip due to? It could be an artifact of the algorithm used to find the jet axis (thrust axis) or could be due to the fact that each particle has been assigned the pion mass, thus underestimating the energy in about 15% of the particles. The authors have used both sphericity and thrust axis as the jet direction and found a difference of less than 10% in the rapidity distributions for $0.1 \leq y \leq 2.0$. They also checked with Monte Carlo that using the wrong mass for kaons and protons does not produce a dip at $y = 0$. Their conclusion is that the dip could be due to string model effects and, to a lesser extent, to an enhancement in the $y = 1.5 - 2$ region due to heavy quark production.

Figure 12 shows recent results from TPC[35] on rapidity distributions measured with respect to the sphericity axis. Figures 12a shows $(1/\sigma_{\rm tot})(d\sigma/dy)$ for all particles, assuming the pion mass. Figures 12b-d show the measured rapidity distributions for pions, kaons and protons obtained using particle identification by dE/dx with the technique described in Ref. 36. They show that the dip at $y = 0$ is present in all distributions, except for that of the protons. The curves were calculated using the LUND[6], Webber[9], Gottschalk[10], and the TUBES[37] Monte Carlo. The discrepancies mentioned earlier (Sec. 2.1.3) are now shown by the curves: the Webber model predicts a softer kaon spectrum, the Gottschalk model predicts too little baryon production. It is clear from Fig. 12 that all models produce a dip at $y = 0$ for pions and kaons, although for each model it has a different origin. The LUND model attributes the dip to string effects in the three-jet events. The Webber model expects such a dip because of soft gluon interference, whereas the Gottschalk model can explain the effect with the kinematics of heavy cluster formation. Certainly part of the effect is due to heavy quark enhancement at $y \sim 2$. Figure 13 illustrates the contributions to the Λ rapidity distribution from different quark flavors. Note that, as for the proton, the LUND model does not predict a dip in the Λ distribution.

It is clear that more detailed analysis is needed to disentangle the different components: light quark fragmentation effects versus heavy quark production. The HRS results discussed by M. Derrick at this Conference, indicate that light quark events exhibit the dip at $y = 0$.

2.2.2 Transverse Momentum Distributions

Fragmentation models fit easily the observed transverse momentum distributions. In the IF model[3-5] limited $p_\perp$ is obtained by giving the individual quarks a Gaussian distributed transverse momentum:

$$\frac{dp}{d_{p_\perp^2}} \sim e^{-p_\perp^2/\sigma_q^2}$$

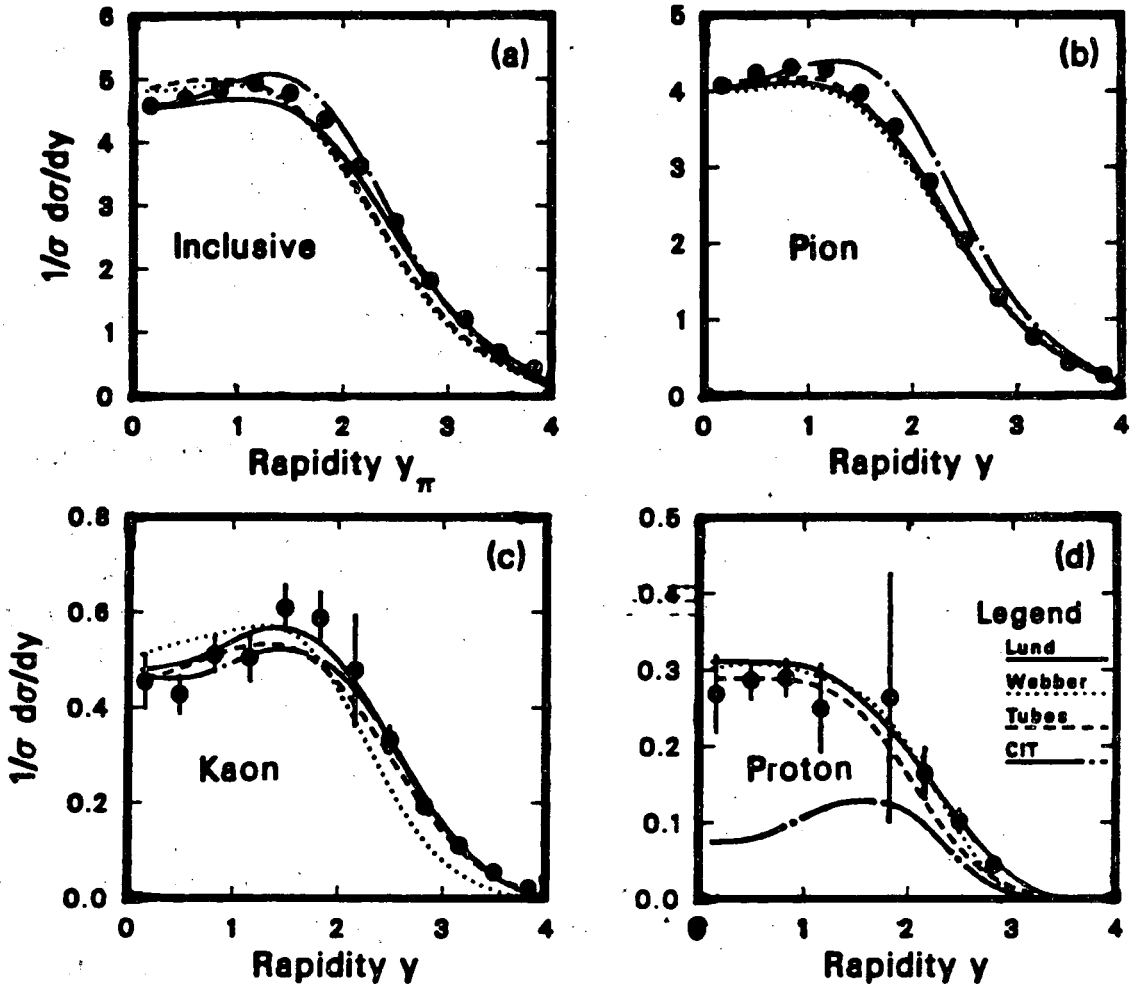

Figure 12: Rapidity measurements reported by the TPC[35]. (a) all particles with pion mass assignment and (b) pion, (c) kaon, (d) proton respectively. The curves are calculated using the models of Ref. 6, 9, 37, and the Gottschalk (CIT) model[10].

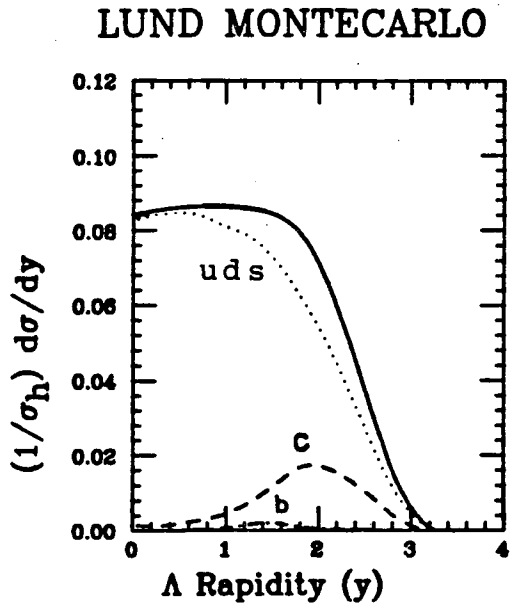

Figure 13: LUND Monte Carlo calculations for the Λ rapidity distribution. The contributions from individual quarks are indicated.

where σ_q is a parameter to be obtained from the data ($\sigma_q \sim .35$ GeV/c). In the LUND model[6] transverse momentum is produced by allowing production of massive quark pairs over some finite length of the confining string. This is viewed as a 'tunnelling phenomenon' and the production probability is:

$$\frac{dp}{dp_\perp^2} \sim e^{-\pi m_\perp^2/k} = e^{-\pi m^2/k} e^{-\pi p_\perp^2/k}.$$

Additional width to the Gaussian distribution in $p_\perp$ is due to soft gluons, and again a parameter, σ_q, will describe the $p_\perp$ distribution. For both models the production of planar events adds a large $p_\perp$ tail to the Gaussian.

New results on transverse momentum distribution have been obtained by the TPC on pions, K^0, protons[38], K^{*0} and ϕ production[22,29]. The results are shown in Figs. 14 and 15. The $p_\perp^2$ distribution for the ϕ compared with the pions is shown in Fig. 14a. The K^{*0} and K^0, again compared with the pion distribution, are shown in Fig. 14b. The curves are in all cases calculated with the LUND model. The following average values are obtained:

particle	$\langle p_\perp^2 \rangle$ (GeV/c)^2	x region
$\pi^\pm$	0.30±0.01±0.02	$x \geq 0.1$
K^0	0.51±0.10±0.18	$0.05 \leq x \leq 0.6$
K^{*0}	0.57±0.07±0.03	$0.0618 \leq x \leq 0.8$
ϕ	1.00±0. 40	$x \leq 0.55$

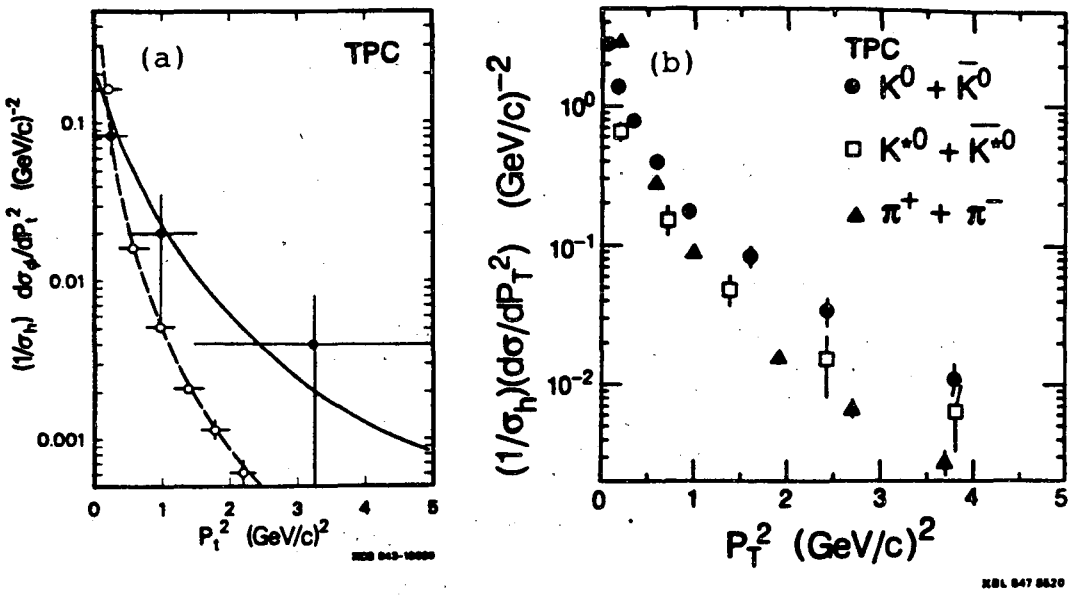

Figure 14: Transverse momentum squared distribution, $p_\perp^2$, for various particles as measured by the TPC. (a) ϕ distribution[29], (b) K^0 and K^{*0} distributions[22]. The pion distribution is included for comparison.

where the first error is statistical, the second systematic. For the ϕ these errors have been added in quadrature. Clearly the K^0, K^{*0} and ϕ distributions indicate a harder spectrum.

Figure 15 shows the proton cross section $(1/\sigma)d\sigma/(dydp_\perp^2)$ for the $\mid y \mid \leq 1$ region. The corresponding pion cross section is also shown for comparison. The proton $p_\perp$ distribution can be represented by a Gaussian shape with $\sigma = 0.55 \pm 0.04$ GeV/c; the full lines represent the prediction of the LUND model.

The LUND model has been tuned to describe the $p_\perp$ distributions of all particles with a $\sigma_q = 0.350$ GeV/c. It is remarkable that, tuned on a mixture of particles (mostly pions), it fits well not only the pions, but also the K^0, K^{*0}, ϕ and proton distributions with no additional assumptions. It should be pointed out that the heavier particles are likely to reflect the $p_\perp$ distribution of primary hadrons, whereas resonance decays soften the observed pion distributions.

The proton $p_\perp$ distribution can also be used to test baryon production mechanisms. If a proton is made out of a diquark and a quark (both of which have the same $p_\perp$ distribution) the proton mean $p_\perp$ is expected to be $\cong \sqrt{2}(p_\perp)_q$. If the proton is made out of three independent quarks (all three having the same mean $p_\perp$), the mean proton $p_\perp$ is expected to be $\cong \sqrt{3}(p_\perp)_q$. Included in Fig. 15 are curves obtained with the LUND Monte Carlo for the diquark-quark case (full lines) and with a modified version of the program emulating the three independent quark

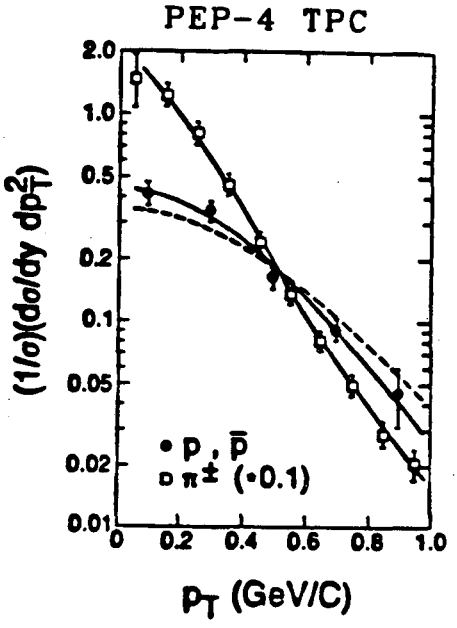

Figure 15: Proton and pion $p_\perp$ distributions for fixed rapidity ($| y | \leq 1$).

hypothesis (dashed lines). The diquark-quark model[23] for the proton fits the data very well. The three-independent-quark model fits the data also, although it appears to be slightly disfavored.

3 PARTICLE CORRELATIONS

The study of two particle correlations in e^+e^- annihilation provides information on the hadronization process. The initial state is a massive virtual photon that decays into a $q\overline{q}$ pair. Within a short time more partons are produced through the mechanisms[3-10] we have discussed in Sec. 1. At a later time these partons are transformed into observable hadrons. Correlations between particles that are far apart in rapidity (LRC) provide information on the initial partons and can test flavor compensation. Correlations between particles that are close in rapidity (SRC) provide information on local conservation of quantum numbers in the fragmentation process.

We review here some new results reported by TASSO[39] and TPC[26] on baryon correlations and by TPC[36] on flavor correlations.

3.1 Baryon Correlations

Baryons are made of three quarks in a color singlet state. In order to understand the mechanism of baryon production, it is important to know if baryon

number is conserved locally, i.e., baryon pairs are produced close in rapidity space or if baryon number is conserved globally, i.e., there is no definite correlation between the baryons produced in a jet. TASSO[39,40] and JADE[40] have reported data on pp and $\bar{p}p$ correlations at low baryon momenta that show evidence for local baryon compensation.

The newer TASSO results[39] are for p and $\bar{p}$ with momentum in the 1–5 GeV/c region. After background subtraction they find the following number of events:

	same jet	opposite jet
pp or $\bar{p}\bar{p}$	1.5 ± 2.1	3.5 ± 2.9
$\bar{p}p$	15.5 ± 4.5	1.2 ± 2.6

in agreement with local baryon number compensation.

The TPC p and $\bar{p}$ results[26] are for low momentum (0.5–1.5 GeV/c) where protons can be identified by dE/dx with backgrounds of at most a few percent. A total of 179 events with a p and a $\bar{p}$ are found. Figure 16a shows the distribution of the angle between the p and the $\bar{p}$. For 107 (72) events the p and $\bar{p}$ are produced in the same (opposite) direction. The curves are quadratic fits to the data: there is a clear excess of events produced in the same jet, as expected for local baryon compensation. Figure 16b shows the opening angle in the plane perpendicular to the jet axis (sphericity axis). The distribution is almost flat in agreement with the TASSO data[40], but in disagreement with the JADE data[40].

The TPC collaboration reports data on Λ-$\bar{\Lambda}$ correlations[26]. In the sample of Λ and $\bar{\Lambda}$ discussed in Sec. 2.1.1 there are fourteen events with two entries. They are divided as follows:

	events	background
$\Lambda - \bar{\Lambda}$	11	1.4 ± 1.2
$\Lambda - \Lambda$	3	2.1 ± 0.9
$\bar{\Lambda} - \bar{\Lambda}$	0	0.6 ± 0.7

where the background was calculated by Monte Carlo simulation and the errors include both statistical and systematic errors. For the Λ-$\bar{\Lambda}$ pairs the distribution of opening angle between the Λ and the $\bar{\Lambda}$ (Fig. 16c) and that of absolute value of rapidity difference, ($|\, dy \,|$ in Fig. 16d), are consistent with local baryon number compensation. For this sample the Λ-$\bar{\Lambda}$ pair multiplicity was calculated to be $0.042 \pm 0.017 \pm 0.014$.

In summary, although none of the above correlation studies have been done with large statistics, there is mounting evidence that the baryon and antibaryon in the event are produced in the same jet. The Λ-$\bar{\Lambda}$ results of the TPC also indicate that the Λ and $\bar{\Lambda}$ are very close in rapidity, which is what is expected for a diquark model mechanism of baryon production. The data have not shown any $p_\perp$ correlations, but since this effect is smeared out by resonance decays this correlation is more difficult to observe.

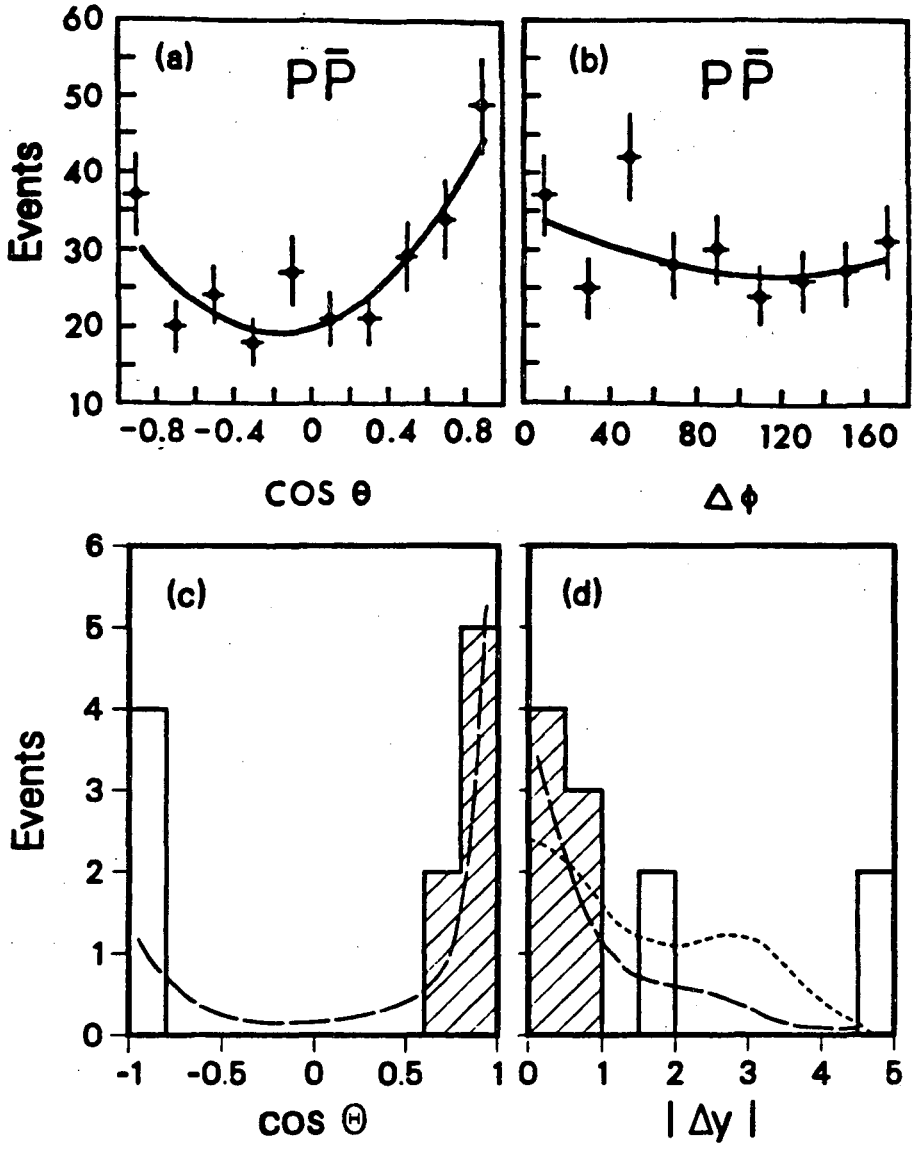

Figure 16: Baryon correlation results of TPC[26]. Opening angle between the p and $\overline{p}$ (a) and Λ and $\overline{\Lambda}$ (c). (b) The angle between p and $\overline{p}$ in the plane perpendicular to the sphericity axis, and (d) the absolute value of the rapidity difference between the Λ and the $\overline{\Lambda}$. The hatched area indicates events in which the Λ and $\overline{\Lambda}$ are in the same jet. The dashed curves in c) and d) are the LUND model predictions.

3.2 Flavor Correlations

TPC, with particle identification over a large solid angle, can study correlations between particles of known flavor[36]. Kaon and pion identification is done by combining dE/dx and momentum measurements, providing a kaon sample with purity $\geq$75% for all rapidity values, and a pion sample with purity $\geq$90%.

The method used is to select a particular quantum number and an interval in rapidity for particles with that quantum number, and then plot the density of other particles in the event weighted by +1 (−1) for the opposite (same) value of that quantum number, as a function of rapidity. The method was first used to investigate charge correlations in hadronic interactions by Drijard et al. in an ISR experiment[41] and later by TASSO in e^+e^- interactions[42]. TASSO reported the observation of long range rapidity correlations (LRC) that provided evidence for the charged nature of primary partons.

A similar technique is used by the TPC collaboration to study $\pi\pi$, KK and Kπ correlations. For each particle in a jet, a rapidity is calculated with respect to the sphericity axis. Then a test particle, a, at a given rapidity, y', is chosen and for all other particles of type b at rapidity y, a charge density is calculated

$$q_a^b(y) = \rho_b^o(y) - \rho_b^s(y)$$

where $\rho_b^o(y)$ ($\rho_b^s(y)$) is the density $(1/\sigma_{tot})d\sigma/dy$ of particles of rapidity y with opposite (same) charge as a. The values of $q_a^b(y)$ versus y, for a test particle in the rapidity interval $y' = 1.5-4$, are plotted in Fig. 17 for the three different cases: $\pi\pi$, KK, πK. The distributions are corrected for acceptance, particle misidentification and radiative effects, using the detector simulation in conjunction with the LUND generator[6]. The corrections are a function of rapidity as well as of the angle of the sphericity axis with respect to the beam line. Error bars in the distributions include the systematic uncertainties associated with these corrections.

The $\pi\pi$ correlations in Fig. 17a are similar to the charge correlations reported by TASSO[42]. There is a large peak (SRC) at about $y = 2$ (the test particle rapidity) due to resonance decays and local charge conservation. A LRC is evident as well: this is evidence for charged primary partons. Integration of the distribution shows that the $\pi^\pm$ charge is compensated by another pion (95$\pm$2)% of the time.

The KK distribution in Fig. 17b is qualitatively similar to that of Fig. 17a for $\pi\pi$. However, the relative strengths of the SRC and the LRC are almost equal, whereas for the $\pi\pi$ case the SRC is stronger than the LRC. For the KK SRC the only known resonance is the ϕ, which, as seen in Table 1, is produced at a significant rate. Using the measured cross section[29], the ϕ contribution to the SRC is extimated to be $\sim$ 20%. It appears therefore that the observed SRC is too large to be explained by resonance decays and is evidence for soft hadronization

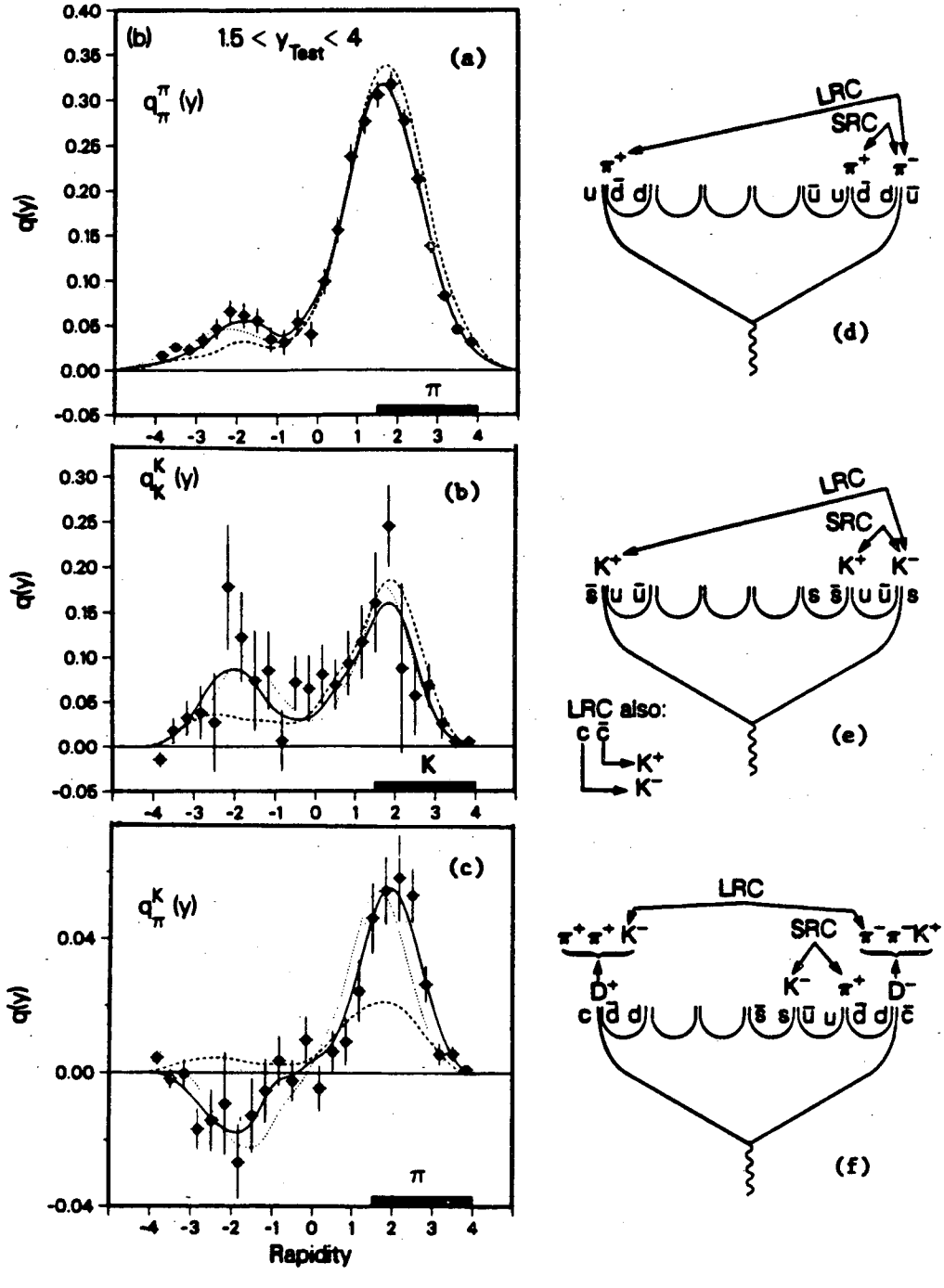

Figure 17: TPC results[36] on flavor-tagged charge density, versus rapidity, y, for (a) $\pi^+\pi^-$, (b) K^+K^- and (c) $\pi^+K^\mp$. The solid (dashed) curves are from the LUND model with (without) c and b quarks. The dotted curves are from the Webber model. (d)–(f) show some mechanisms responsible for LRC and SRC.

and local strangeness compensation. The LRC are due to primary $c\bar{c}$ and $s\bar{s}$ quarks, as indicated in Fig. 17e.

Finally, the Kπ correlation of Fig. 17c illustrates the effect of heavy quark decays. The LRC shows a significant same-sign charge correlation. This can be explained with charm production as illustrated in Fig. 17f. The curves drawn in Fig. 17c are the predictions of the LUND model (solid line), of the same model without heavy c and b quarks (dashed line) and of the Webber model (dotted line). It is clear that most of the observed SRC and LRC are due to heavy quarks. The Webber model and the LUND model agree with the data for all cases: $\pi\pi$, KK and Kπ. It is not possible to distinguish between these two models with the information contained in these graphs.

In conclusion, short and long range flavor correlations have been observed by the TPC collaboration. Short range correlations indicate that quantum numbers are locally conserved. Long range correlations show that the primary quarks carry flavor and that heavy quarks produce sizable effects.

4 TEST OF FRAGMENTATION MODELS: "THE STRING EFFECT"

The fragmentation models we have used describe most features of the data equally well. There are a few exceptions (Sec.2.2): the Webber model gives too soft a kaon distribution, and the Gottschalk model gives too few protons. These are discrepancies well known to the authors of these models and can probably be eliminated without fundamental changes to the models.

Is there any feature of the data that can point out fundamental differences among the models? JADE[11] has studied three-jet events and reported evidence that in certain angular regions the LUND model[6] represents the data better than the independent fragmentation (IF) model[3-5]. New data on this subject are reported at this Conference by TPC and by JADE. We will discuss the TPC results, the JADE results are discussed in the paper presented by A. Petersen[43].

Figure 18 illustrates the difference between the IF and the LUND fragmentation models for 3-jet events. In the IF model all partons fragment independently, therefore each jet is symmetric with respect to its jet axis (Fig. 18b). In the LUND model, the gluon is a kink in the string connecting the q and $\bar{q}$ and fragmentation proceeds along the dashed lines in Fig. 18a. The two string segments qg and $\bar{q}g$ fragment independently in a symmetric way in their own center-of-mass. Then, when the particles are boosted in the overall center-of-mass, they are pulled in the gluon direction depleting the region between the q and the $\bar{q}$. The particle densities in the region between the q and the $\bar{q}$ are therefore expected to be lower for the LUND model than for the IF model. In addition, the effect of the boost is expected to be stronger for particles with larger tranverse mass $m_\perp = \sqrt{p_\perp^2 + m^2}$, since the

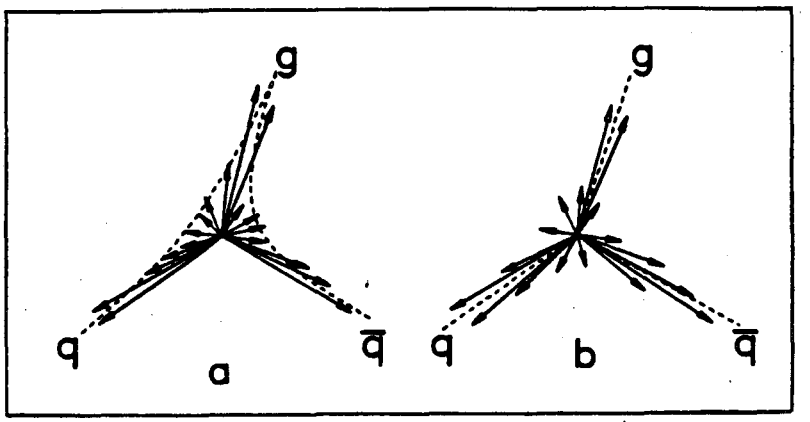

Figure 18: Illustration of the difference between the IF[3-5] and the LUND[6] models for three-jet events. In the LUND model (a), the fragmentation is along strings stretched between the partons; in the IF model (b), the fragmentation is along the parton direction.

$\mathbf{p} \cdot \mathbf{n}_B$ component along the boost ($\mathbf{n}_B$) is changed as $\mathbf{p} \cdot \mathbf{n}_B = \gamma_B(\mathbf{p} \cdot \mathbf{n}_B - \beta_B E)$. JADE[11] observed these effects by studying three samples of data: all particles, kaons, and particles with transverse momentum component out of the event plane $p_{\text{out}} \geq 0.3$.

New analysis from the TPC confirms these results and goes further in testing the string hypothesis. In addition they report that the data are also well fit by the Webber model.

4.1 Tests of the string model: TPC results

The procedure used by the TPC Collaboration[44,45] to test fragmentation models is as follows: a. optimize the IF and LUND model parameters to fit the data as a whole (both 2-jet and 3-jet events), b. select 3-jet events and study particle densities comparing with models, c. vary the treatment of the gluon and the energy-momentum conservation in the IF model to verify that infact the results are not dependent upon the particular treatment used.

To test the IF and the LUND models, TPC uses the LUND Monte Carlo program that provides options to run the IF model with different gluon modelling and different energy-momentum conservation schemes (the IF model cannot conserve energy and momentum simultaneously). The initial choice for the IF model is a gluon a la Hoyer[4] i.e., the gluon fragments like a quark and energy-momentum is conserved as to conserve parton direction. The LUND program used[6] includes second-order QCD and the 'symmetric' fragmentation function (JADE used first-

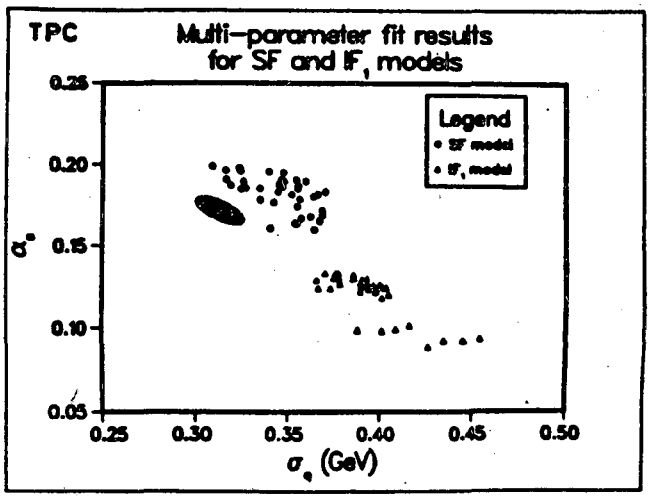

Figure 19: Results of the TPC[45] fit of the data to the IF[3-5] and LUND[6] (SF) fragmentation models. The values obtained for σ_q versus α_s are shown for the 40 different fits (see text). The IF results concentrate on the lower right. The solid black point indicates the typical 1σ statistical error.

order and the 'standard' fragmentation):

$$f(z) = e^{-bm_\perp^2/z}(1-z)^a/z.$$

Here z is the fraction of available energy-momentum taken by the hadron, $m_\perp$ is the transverse mass, and b and a are parameters to be determined from the data. TPC only fits a and fixes b to $b = 0.6$ which gives a good fit to the measured D* fragmentation function. The three parameters to be determined are a, σ_q and α_s. To determine these parameters, eleven different distributions (n_{ch}, $D(x)$, aplanarity, thrust, $\langle p_\perp \rangle_{\text{in}}$, $\langle p_\perp \rangle_{\text{out}}$, etc.) are used, divided in sets depending whether they are sensitive to a, σ_q or α_s. There are two distributions in the set for a, four for σ_q, and five for α_s. This gives a total of $2 \times 4 \times 5 = 40$ combinations of the distributions that could give 40 predictions for the parameters. These multiple predictions are used to estimate the systematic error associated with the parameters' determination. Figure 19 shows the 40 solutions for the IF and SF (string fragmentation, LUND model). There is a clear separation between the two sets of solutions, the IF giving systemetrically lower values of α_s and lower value of σ_q as expected. The results are

a	σ_q	α_s	
$1.23 \pm .12$	$.390 \pm .018$	$.125 \pm .013$	IF
$0.955 \pm .100$	$.350 \pm .016$	$.183 \pm .010$	LUND

where the errors include both statistical and systematic contributions. Both models give reasonably good fits to the data. The TPC results agree with similar trends observed by TASSO and CELLO[46] and discussed by T. Sjostrand[47]. The different values for these parameters are related to the fragmentation mechanism. The LUND model, in going from the string center-of-mass to the overall center-of-mass, tends to smear the jet structure; some 3-jet events look like 2-jet events, so it needs a larger value of α_s to compensate.

The 3-jet events are then selected using the sphericity eigenvalues, Q_1, Q_2, Q_3 (defined in increasing order). Both charged and neutral particles are used to find S. Planar 3-jet events are selected by requiring $Q_1 \leq 0.06$ and $Q_2 - Q_1 \geq 0.05$, in addition to other cuts to assure uniform acceptance for the 3-jets. A sample of 3022 events is so obtained. Jets are labelled 1, 2, and 3 according to the angles between them: jet 1 is opposite to the smallest angle, jet 3 is opposite to the largest angle and is expected to be preferentially the gluon jet. The coordinate system is chosen as to have $\phi = 0$ in the direction of jet 1.

Figure 20 shows the particle flow $(1/N)dN/d\phi$ for three different samples: a. charged particles and photons, b. same particles but requiring $0.3 \leq p_{\text{out}} \leq 0.5$ and c. heavy particles. The curves are from the IF, LUND (SF) and Webber (CF) model. The region between jets 1 and 2 is depleted with respect to the IF model in all three distributions. the data agree very well with the LUND model in all cases. The IF model overpredicts the particle density in the 1-2 valley by about 30% in Fig. 20a and by a factor 2 in the case of heavy particles (Fig. 20c). For the Webber model the predictions in all the valleys are a little larger than the data, however this result is sensitive to the parameters used and can be attributed to lack of tuning.

In order to quantify the agreement of the data with the Monte Carlo, a ratio of particles between jets 3-1 and jets 1-2, is calculated $r = N_{31}/N_{12}$. N_{ij} is defined as the number of particles between jet i and j in the angular region such that $(\phi_{\text{particle}} - \phi_i)/(\phi_j - \phi_i) = 0.3 - 0.7$. This angular region is the most sensitive to string effects. The ratio N_{31}/N_{12} is shown in Fig. 21 for the data and the models. For the IF model this ratio is ~ 1 in all cases. For the data, the LUND and the Webber models the ratio is significantly higher than 1. The value of N_{31}/N_{12} increases with p_{out} (Fig. 21b) and with increasing mass (Fig. 21d) as expected. The surprise is that the Webber model predicts this effect as well; its origin will be discussed in the next section.

Finally, the TPC group has investigated in detail whether the IF model can be tuned to reproduce the observed dip in the jets 1-2 valley and its p_{out} and mass dependence[45]. Different gluon fragmentation and different energy-momentum conservation schemes have been tried. In total, six different cases were tried, obtaining a variety of best fit values for a, σ_q and α_s. Regarding the dip in the jets 1-2 valley the results were quite similar to the case shown in Figs. 20 and 21.

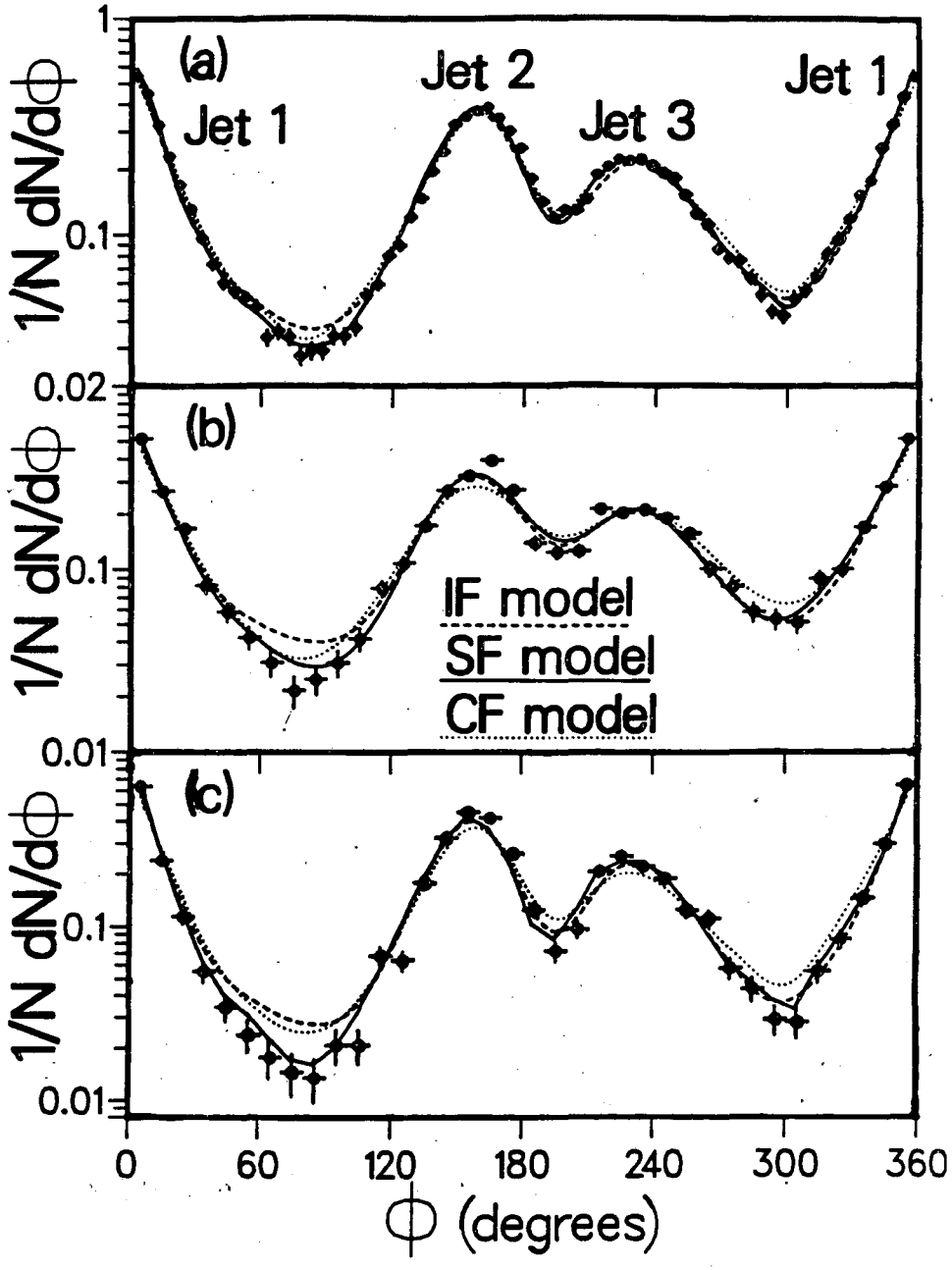

Figure 20: TPC results[44] n particle flow $(1/N)dN/d\phi$ for (a) all charged particles and photons, (b) same as (a) but with $0.3 \leq p_{out} \leq 0.5$ and (c) heavy particles (K^0_S, $K^{\pm}$, p and Λ).

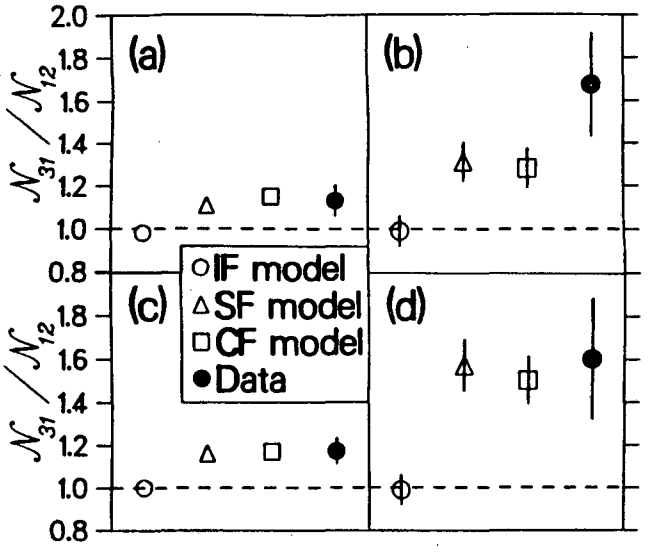

Figure 21: The ratio N_{31}/N_{12} of normalized particle densities between jets from the TPC analysis[44] for the data and the models. (a) charged pions with $0.0 \leq p_{out} \leq 0.2$, (b) charged pions with $0.3 \leq p_{out} \leq 0.5$, (c) all charged pions, and (d) heavy particles (K^0_s, $K^{\pm}$, p, Λ).

The conclusion is that the failure to fit this feature of the data is a fundamental flaw of the IF model.

4.2 The Webber model and the 'string effect.'

The Webber model is based on a parton shower generated using the leading-log approximation of QCD. It includes soft gluon interference effects that lead to angular ordering of successive gluon emissions[9,17]. This angular ordering, as pointed out by B. Webber at this Conference, is at the origin of the observed string-like effects. This is illustrated in Fig. 22, which is a schematic representation of a $q\bar{q}g$ event. The gluons are represented by double lines, the quarks by single lines. Because of angular ordering, the gluons emitted after the first one will tend to be emitted in the direction of the initial partons. Clusters will form between jets 1-3 and 2-3 to locally neutralize the color charges. This is indicated by the dotted elipses. The end result is a depletion of clusters between jets 1-2. This effect is still present after cluster decays into hadrons, although it is partially smeared out by phase space decays.

The TPC group has also investigated whether a string-like effect is present in the Gottschalk model[10] and in all cases found $N_{31}/N_{12} \sim 1$. This model does not include gluon interference which leads to angular ordering as the Webber model and has no other mechanism, as of now, that could produce such an effect.

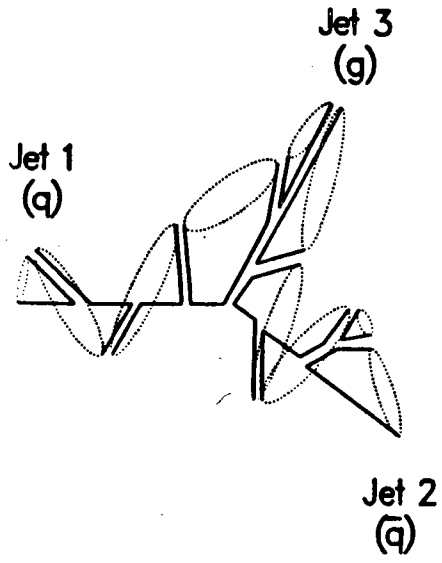

Figure 22: Schematic of a 3-jet event in the Webber model. Quarks are represented by single lines, gluons by double lines. The dotted elipses represent clusters (see text).

In conclusion, there are two models (LUND and Webber) that explain the depletion of particle density between jets 1-2. These models are very different, as discussed in the Introduction, therefore it is very surprising that they both can explain such a detail in the event structure. Obviously some other type of data is needed to distinguish between these two models.

5 SUMMARY

A lot of new data have been reported since the 1983 Conference on Multiparticle Dynamics. These can be summarized as follows.

Particle content in jets and fragmentation functions for many resonant states have now been measured: data on K^{*0}, $K^{*\pm}$, ϕ and new data on ρ meson have been reported.[22,29-32])

These distributions are in general harder than those of stable particles (mostly products of resonance decays), giving information that is closer to the hadronization process. The LUND model[6]) is able to fit multiplicities, fragmentation functions and transverse momentum distributions with no additional parameters.

The added knowledge on vector meson production allows measurements of the vector to pseudoscalar production ratio, a parameter in conventional models.

It seems clear that for heavy quarks this ratio is close to 3/1, whereas for light quarks it is close to 1/1.

Rapidity distributions for individual particles from TPC[35] and for a selected light quark sample (see M. Derrick talk at this Conference) may shed some light on the observed dip at $y = 0$.

New results have been presented on two particle correlations, that are expected to provide deeper understanding of the fragmentation process. Local baryon compensation has been observed in $\overline{p}-p$ and $\Lambda-\overline{\Lambda}$ production[26,39]. Flavor correlations have been studied by the TPC[36]. Both short-range and long-range flavor compensation are observed in the $\pi\pi$, KK, and Kπ charge-weighted rapidity correlations. Short range correlations indicate that quantum numbers are locally conserved. Long range correlations show that the primary quarks carry flavor and that heavy quarks produce sizable effects.

Finally, string-like effects predicted by the LUND model[6] have been observed by JADE[11,43] and confirmed by TPC[44]. The observed effect is a depletion of particles between the jets produced by the two quarks in $q\overline{q}g$ events. This effect cannot be explained by the conventional Independent Fragmentation model[3-5]. The surprising result discussed at this Conference is that the Webber QCD-Cluster model, based on a completely different approach to fragmentation, also predicts this effect. It is a challenge to the experimentalists to find some other features of the data that can distinguish between models or, perhaps, to the theorists to understand why models that look so fundamentally different produce the same results.

REFERENCES

1. G. Hanson et al., Phys.Rev.Lett 35, 1609 (1975).

2. R.Brandelik et al. (TASSO), Phys.Lett. 86B, 243 (1979); D.P. Barber et al. (MARK I), Phys.Rev.Lett. 43, 830 (1979); Ch. Berger et al. (PLUTO), Phys.Lett. 86B, 418 (1979); W. Bartel et al. (JADE), Phys.Lett. 91B, 142 (1980); H.J. Behrends et al. (CELLO), Phys.Lett. 110B, 329 (1982).

3. R.D. Field and R.P. Feynman, Phys.Rev. D15, 2590 (1977); Nucl.Phys. B138, 1 (1978).

4. P. Hoyer et al., Nucl.Phys. B161, 349 (1979).

5. A. Ali et al., Phys.Lett. 93B, 155 (1980); Nucl.Phys. B167, 454 (1980).

6. B. Andersson, G. Gustafson, G. Ingelman and T. Sjostrand, Phys. Reports 97, 31 (1983); also T. Sjostrand, Comp.Phys.Com. 27, 243 (1982) and 28, 229 (1983). We use the 'symmetric' LUND model (JETSET 5.2), with

parameters: u/s=3/1; V/p=1/1 for light quarks and 3/1 for heavy quarks; $\alpha_s = .183, \sigma_q = 0.350$ GeV, and fragmentation parameters a = .955 and b = 0.6.

7. G.C. Fox and S. Wolfram, Nucl.Phys. B168, 285 (1980); R.D. Field and S. Wolfram, Nucl.Phys. B213, 65 (1983).

8. R. Odorico, Nucl.Phys. B172, 157 (1980); P.Mazzanti and R. Odorico, Z.Physik C7, 61 (1980).

9. B.R. Webber, Nucl.Phys. B238, 492 (1984), see also B.R. Webber, these Proceedings. We use the following values of the parameters: QCD scale $\Lambda = 0.30$ GeV, gluon mass cut-off $Q_0 = 0.70$ GeV and mass threshold above which clusters are no longer isotropic $M_f = 3.5$ GeV.

10. T.D. Gottschalk, Nuc.Phys. B214, 201 (1983); B239, 325 (1984); B239, 349 (1984); also Caltech preprints CALT-68-1059 (1983) and CALT-68-1083 (1984). The parameters corresponding to the March 1984 programs are: $t_c = 25$ GeV^2, $W_{max} = 4$ GeV, $\rho_c = 2.5$ GeV^{-2}, $W^c_{min} = 0.5$ GeV.

11. W. Bartel et al. (JADE), Phys.Lett. B134, 275 (1984). See also A. Petersen, these Proceedings.

12. D. Bender et al. (HRS), 'Study of Quark Fragmentation at 29 GeV: Global Jet Parameters and Single Particle Distributions,' ANL-HEP-PR-84-08 (May 1984), submitted to Phys.Rev.D.

13. R. Brandelik et al. (TASSO), Phys.Lett. 114B, 65 (1982); Althoff et al. (TASSO), Z. Physik C22, 307 (1984).

14. H. Aihara et al. (TPC), Phys.Rev.Lett. 52, 577 (1983).

15. M. Althoff et al. (TASSO), Z.Physik C17, 5 (1983); M. Althoff et al. (TASSO), to be published.

16. A.H. Mueller, Phys.Lett. 104B, 161 (1981); Ya.L. Dokshitzer et al., Phys.Lett 115B, 242 (1982), also Z.Phys. C18, 37 (1983); A. Bassetto et al., Phys.Rep. 100, 202 (1983); L.V. Gibov et al., Phys.Rep. 100, 1 (1983).

17. G. Marchesini and B.R. Webber, Nucl.Phys. B238, 1 (1984). See also G. Marchesini in these Proceedings.

18. H. Aihara et al. (TPC), 'Inclusive γ and π^0 Production in e^+e^- Annihilation at 29 GeV,' LBL-18326 (Sept. 1984), to be published.

19. R. Brandelik et al. (TASSO), Phys.Lett. 108B, 71 (1982); H.J. Behrend et al. (CELLO), Z.Physik C20, 207 (1983).

20. W. Bartel et al. (JADE), Phys.Lett. 130B, 454 (1983).

21. R. Brandelik et al. (TASSO), Phys.Lett. 94B, 91 (1980); N_{K^0} quoted here is from S.L. Wu, DESY 83-007 (1983) and Proceedings of the Summer Inst. on Particle Physics, Ed. by A. Mosher, SLAC (1982), p. 555. W. Bartel et al. (JADE), Z.Physik C20, 187 (1983).

22. H. Aihara et al. (TPC), 'K*0 and K^0 Meson Production in e^+e^- Annihilation at 29 GeV,' LBL Report LBL-18325, (Sept. 1984), to be published.

23. E.M. Ilgenfritz et al., Acta Phys.Polon. B9, 881 (1978); S. Ritter and J. Ranft, Acta Phys.Polon B11, 259 (1980); A. Bartl et al., Z. Physik C6, 335 (1980); A. Bartl et al., Phys.Rev. D6, 1061 (1982); A. Bartl et al., Phys.Lett. 122B, 427 (1982); B. Andersson et al., Nucl. Phys. B197, 45 (1982).

24. T. Meyer, Z. Physik C12, 77 (1982).

25. M. Brandelik et al. (TASSO), Phys. Lett. 105B, 75 (1981); W. Bartel et al. (JADE), Phys.Lett. 104B, 325 (1981).

26. K. Maruyama (TPC), University of Tokyo preprint UT-HE-84/09 to appear in Proceedings of the 1984 Recontre de Moriond; H. Aihara et al. (TPC), 'Λ Production in e^+e^- Annihilation at 29 GeV', LBL Report LBL-18382 (Sept. 1984) to be published.

27. M. Althoff et al. (TASSO), Phys.Lett. 130, 340 (1983).

28. R. Brandelik et al. (TASSO), Phys.Lett. 117B, 135 (1982).

29. H. Aihara et al. (TPC), Phys.Rev.Lett. 52, 2201 (1984).

30. DELCO collaboration, presented at the Vanderbilt Conference on e^+e^- (April 1984).

31. J.A. Kadyk (MARK II), presented at the Leipzig Conference (1984); also H.M. Schellman (MARK II), Lawrence Berkeley Laboratory thesis (in preparation).

32. W. Bartel et al. (JADE), 'Inclusive Production of Vector Mesons ρ^0 and K*± in e^+e^- annihilation at $\sqrt{s} = 35$ GeV,' DESY Report DESY-84-58 (1984).

33. M. Althoff et al. (TASSO), Phys.Lett. 126B, 493 (1983); S. Ahlen et al. (HRS), Phys.Rev.Lett. 51, 1147 (1983) and presented at this Conference (see J. Izen talk); J.M. Yelton et al. (MARK II), Phys.Rev.Lett. 49, 430 (1982); W.Bartel et al. (JADE), DESY Report DESY-84-059 (1984).

34. M. Althoff et al. (TASSO), Phys.Lett. 136B, 130 (1984).

35. M.D. Shapiro (TPC), 'Inclusive Rapidity Distributions,' TPC Note TPC-LBL-84-43 (1984), to be published.

36. A. Aihara et al. (TPC), 'Observation of Strangeness Correlations in e^+e^- Annihilation at $\sqrt{s} = 29$ GeV,' LBL Report LBL-18125 (August 1984), to be published.

37. C.T. Day, 'TUBES Monte Carlo: User's Guide,' Lawrence Berkeley Laboratory Report TPC-LBL-81-27 (1981); The hadronization mechanism of this Monte Carlo is similar to the LUND one, although developed independently. It offers flexibility in changing particle decay branching ratios.

38. H. Aihara et al. (TPC), Phys.Rev.Lett. 53, 130 (1984).

39. M. Althoff et al. (TASSO), Phys. Lett. 139B, 126 (1984).

40. W. Bartel et al. (JADE), Phys.Lett. 104B, 325 (1981); M. Althoff et al. (TASSO), Z. Physik C17, 5 (1983).

41. D. Drijard et al. (ACCDHW), Nucl.Phys. 166B, 233 (1980).

42. R. Brandelik et al. (TASSO), Phys.Lett. 100B, 357 (1981).

43. A. Petersen (JADE), 'Further Studies on Quark and Gluon Fragmentation', talk presented at this Conference

44. H. Aihara et al. (TPC), 'Test of Models for Parton Fragmentation using 3-Jet Events in e^+e^- Annihilation at $\sqrt{s} = 29$ GeV', LBL Report LBL-18407 (1984).

45. H. Aihara et al. (TPC), 'Tests of Models for Quark and Gluon Fragmentation in e^+e^- Annihilation at $\sqrt{s} = 29$ GeV', LBL Report LBL-18408 (1984).

46. Behrends et al. (CELLO), Phys.Lett. 138B, 311 (1984); M. Althoff et al. (TASSO), DESY Report DESY 84-057 (June 1984).

47. T. Sjostrand, 'Some Comments on Jet Fragmentation Models and α_s determinations', DESY Report DESY 84-023 (1984).

This report was done with support from the Department of Energy. Any conclusions or opinions expressed in this report represent solely those of the author(s) and not necessarily those of The Regents of the University of California, the Lawrence Berkeley Laboratory or the Department of Energy.

Reference to a company or product name does not imply approval or recommendation of the product by the University of California or the U.S. Department of Energy to the exclusion of others that may be suitable.

TECHNICAL INFORMATION DEPARTMENT
LAWRENCE BERKELEY LABORATORY
UNIVERSITY OF CALIFORNIA
BERKELEY, CALIFORNIA 94720